



**HAL**  
open science

## CoSb<sub>3</sub>-Based Thin-Film Thermoelectric Devices with High Performance Via Electrode Optimization

Dongwei Ao, Fu Li, Yuexing Chen, Jingting Luo, Guangxing Liang,  
Zhuanghao Zheng, Xianghua Zhang, Ping Fan

► **To cite this version:**

Dongwei Ao, Fu Li, Yuexing Chen, Jingting Luo, Guangxing Liang, et al.. CoSb<sub>3</sub>-Based Thin-Film Thermoelectric Devices with High Performance Via Electrode Optimization. ACS Applied Energy Materials, 2021, 4 (5), pp.5265-5273. 10.1021/acsaem.1c00795 . hal-03268309

**HAL Id: hal-03268309**

**<https://hal.science/hal-03268309v1>**

Submitted on 15 Jun 2023

**HAL** is a multi-disciplinary open access archive for the deposit and dissemination of scientific research documents, whether they are published or not. The documents may come from teaching and research institutions in France or abroad, or from public or private research centers.

L'archive ouverte pluridisciplinaire **HAL**, est destinée au dépôt et à la diffusion de documents scientifiques de niveau recherche, publiés ou non, émanant des établissements d'enseignement et de recherche français ou étrangers, des laboratoires publics ou privés.

# CoSb<sub>3</sub> based thin film thermoelectric devices with high performance via the electrode optimization

Dongwei Ao <sup>a,b</sup>, Fu Li <sup>a</sup>, Yuexing Chen <sup>a</sup>, Jingting Luo <sup>a</sup>, Guangxing Liang <sup>a</sup>, Zhuanghao Zheng <sup>a,\*</sup>, Xiang-Hua Zhang <sup>c</sup>, Ping Fan <sup>a</sup>

<sup>a</sup> Shenzhen Key Laboratory of Advanced Thin Films and Applications, Key Laboratory of Optoelectronic Devices and Systems of Ministry of Education and Guangdong Province, College of Physics and Optoelectronic Engineering, Shenzhen University, Shenzhen 518060, P. R. China

<sup>b</sup> School of Materials Science and Engineering, Hanshan Normal University, Chaozhou 521041, People's Republic of China

<sup>c</sup> Univ Rennes, CNRS, ISCR (Institut des Sciences Chimiques de Rennes) UMR6226, Rennes F-35000, France.

\* Corresponding authors E-mail: [zhengzh@szu.edu.cn](mailto:zhengzh@szu.edu.cn)

**Abstract:** Flexible thin film thermoelectric devices have been extensively studied for powering wearable electronics and particularly as power source for self-powered sensors or temperature detection. The skutterudite CoSb<sub>3</sub> is emerging as one of the most studied candidate materials for thermoelectric applications. This work is focused on the a comprehensive optimization in terms of CoSb<sub>3</sub> based thin films as well as the electrode materials and structure with the objective to fabricate high performance flexible device. The CoSb<sub>3</sub> based thin films with nanoparticles for the enhancement of phonon scattering have been fabricated by using vacuum sputtering method. N-type and P-type thin films can be obtained by appropriate doping with Ti and In, respectively. It has been demonstrated that a multilayer structure of the electrodes can

greatly enhance the thermoelectric performance of the thermoelectric device by increasing the output power and the thermal stability of the device in the air atmosphere. It has also been demonstrated the possibility of obtaining a relatively high output voltage of above 90 mV and a high-power density of 0.46 mW/cm<sup>2</sup> at a current intensity of about 0.35 mA with the device. Therefore, many applications can be considered. The thin-film thermoelectric device has also been tested as thermal sensor and exhibits fast responsivity, with a reaction time of a few hundreds of milliseconds, as well as high stability.

**Keywords:** Flexible; CoSb<sub>3</sub>; Electrode; Thin film; Thermoelectric device;

## 1. Introduction

Solid-state thermoelectric (TE) device is capable of converting waste heat into electricity depending on the temperature interval in which its efficiency peaks [1]. It can be widely used in the field of energy sources, semiconductor cooling and temperature sensor due to its extensive advantages such as no moving parts, silent, high reliability, and autonomous operation [2]. The efficiency of TE device is directly related to the dimensionless thermoelectric figure of merit,  $ZT = S^2\sigma T/\kappa$  (Seebeck coefficient  $S$ , electrical conductivity  $\sigma$ , the absolute temperature  $T$  and total thermal conductivity  $\kappa$ , where  $\kappa = \kappa_{lat} + \kappa_{ele}$  that  $\kappa_{lat}$  is lattice thermal conductivity and  $\kappa_{ele}$  is electrical thermal conductivity) [3]. Recently, the increasing demand of micro-scale energy harvesting for power supply or miniaturization sensor provides an opportunity for the investigation of the multifunctional flexible TE (f-TE) devices, which have the advantages of flexibility, small volume, light weight, high integration, and enhanced compatibility [4]. For instance, Kim et al. [5] demonstrated that a wearable

thermoelectric generator fabricated on a glass fabric, can use the human body as heat source with stable output power. Culebras et al. [6] reported a low-cost flexible thermoelectric generator based on organic materials as a low-power source. However, there are still several challenges remaining for f-TE application; (a) Increase the thermoelectric efficiency at low temperature where the f-TE is generally supposed to be used. Despite many promising materials with high ZT value even higher than 2, obtained by using many available methods in the past decades [7-10]), but most of those materials still have low efficiency at the temperature below 250 °C where the majority of the waste heat reserves is located. (b) The second challenge is to conserve the thermal stability. Generally, the performance of the materials in the f-TE, including organic or inorganic thermoelectric materials and the bonding electrodes, will be changed during the operated process, typically turning worse due to the increasing thermal stress and oxidation effect after bending, temperature increasing or using in the air atmosphere; (c) The last challenge is to reducing the preparation cost. Actually, the high cost of preparing f-TE device is not only because of the unaffordable or toxic element of the materials (such as TE materials containing Te, Pb, Se, PEDOP and electrode materials of Au, Ag), but also its slow and complicated preparation process. Indeed, for the targeted applications with low power consumption, providing a low-cost f-TE device with an acceptable performance is even more important than preparing a high-performance device with a high production cost.

Among various reports about the flexible devices, which aim at addressing these limitations [11-14], generator based on thin films have attracted increasing attention for f-TE application. Previous studies indicate that the thin films with nanostructure can be used to control the phonon transport by the quantum confinement effect which

can enhance the ZT value, leading to the enhancement of the conversion efficiency [15-18]. For instance, Venkatasubramanian et al. [15] achieved a very high ZT of  $\sim 2.4$  using  $\text{Bi}_2\text{Te}_3\text{-Sb}_2\text{Te}_3$  quantum well superlattice structure with a periodicity of 6 nm. With the same principle of concept, Chowdhury et al. [19] made a device fabricated from  $\text{Bi}_2\text{Te}_3$ -based superlattices into state-of-the-art electronic packages and cooling with a high ( $\sim 1,300\text{Wcm}^{-2}$ ) heat flux; Tian et al. [20] prepared a organic suprelattices generator with very high power density of  $2.5\text{ Wm}^{-2}$  which is almost one hundred times higher than the others. On the other hand, some emerging advantages of thin film f-TE (tf-TE) device can provide new opportunities for TE application. Typically, it can be directly integrated into micro-scale devices and packaged in macro-scale systems. For examples, Yadav et al. [21] has integrated a thermoelectric power generator into a fiber by vacuum evaporation, which can directly convert the body heat to electricity for wearable devices. Szobolovszky et al. [22] designed and embedded flexible thermoelectric generators into high power light emitting diode (LED). The available thermal gradient of approximately 50 K allows conversion of the LED waste heat with an overall efficiency of 1%. Importantly, the tf-TE device has a faster response speed than those formed by bulk materials due to their smaller thickness and special surface electric transmission [23-25]. For examples, Deng et al. [23] and Pan et al. [24] presented the hybrid detector with very short response time for visible and near-infrared light. In addition, due to the feature of larger length to area ratio for tf-TE legs and easier preparation method, a variety of device structure is feasible, such as forming in-plane structure to achieve large temperature gradient for maximum output power [24], and fabricating cross-plane device with low internal resistance for high cooler efficiency [25]. For these reasons, the tf-TE devices have been considered as essential for TE applications.

Skutterudite  $\text{CoSb}_3$  has drawn extensive attention as one of the most promising thermoelectric materials in the intermediate temperature range [26-28]. Some significant reports [29-34] indicated that the  $\text{CoSb}_3$  can obtain high ZT value as both P-type and N-type materials with comparable characteristics, making much easier to find electrode material for preparing homojunction device structure. Thus, it is favorable to fabricate highly efficient and low-cost TE generators based on  $\text{CoSb}_3$ .

Hence, in this paper, a complete  $\text{CoSb}_3$  based tf-TE device will be fabricated by using vacuum sputtering, which is a low-cost and mass-production compatible technique for assuring thin films performance. The emphasis will be on the comprehensive optimization of the  $\text{CoSb}_3$  base tf-TE device in terms of TE material, electrode, and device integration. Filling element and nanostructure evolution are adopted to improve the performance of the P-type and N-type  $\text{CoSb}_3$  thin films. Then, the optimization of electrode design for the TE thin films connecting will be realized with the multilayer strategy. The thermoelectric generation performance will be characterized, followed by a feasibility study as body detection sensor.

## **2. Experimental**

### ***Thin films growing***

The N-type In-doped  $\text{CoSb}_3$  and P-type Ti-doped  $\text{CoSb}_3$  nano thin films were synthesized by magnetron sputtering. Ti target (99.99 %), In target (99.99 %) and  $\text{CoSb}_3$  (99.95%) alloy target was used in a magnetron sputtering facility, equipped with a three-position rotatable target system. We chose the Kapton type polyimide (PI) with the thickness of 0.15 mm and the thermal conductivity of  $0.35 \text{ Wm}^{-1}\text{K}^{-1}$  as the substrate, which has excellent heat resistance. A schematic representation of the process is shown in Figure 1 (a) and (b). The nanostructure In-doped  $\text{CoSb}_3$  was prefabricated by multilayer approach as shown in Figure 1 (a) and the experimental

details were reported in our previous work [35]. As shown in Figure 1 (b), the P-type Ti-doped  $\text{CoSb}_3$  nano thin film was fabricated by pre-deposited layer approach through layer inter-diffusion. Firstly, Ti layer was deposited on the PI substrate with a very low deposition rate of around  $0.3 \text{ \AA/s}$  and the thicknesses was controlled to be around 20 nm. Then, the  $\text{CoSb}_3$  thin film was deposited onto the Ti layer by using the same parameters for preparing N-type thin film, followed by a thermal annealing (at  $300 \text{ }^\circ\text{C}$ ) in a furnace under constant flow of argon.

### ***Fabrication of tf-TE device***

Figure 1 illustrates also the process for preparing tf-TE device. Based on our previous research results [35, 36], In- and Ti-doped  $\text{CoSb}_3$  achieved the best TE performance by using a multilayer method and a pre-deposited layer method, respectively. At first, the P-type thin film “leg” was deposited on the PI substrate and then the N-type thin film “leg” with the similar thickness was deposited, followed by a thermal annealing process. Thirdly, the P-type and N-type thin films are connected by the metal layer as shown in Figure 1 (c). The Cu, Al, Mo and Ni were chosen as the electrode materials and all of them were prepared by direct magnetron sputtering with a thickness about 300 nm. The optimization of the electrode structure, shown in Figure 1 (c), will be realized after investigating the influence of the electrode materials on the connecting efficiency of the device. Figure 1(d) shows the image of the device.

### ***Sample characterization and device performance measurement***

The crystalline phases were characterized by X-ray diffraction technique (D/max2500) using Cu  $K_\alpha$  radiation ( $\lambda = 0.15406 \text{ nm}$ ). The micro-structure was examined by scanning electron microscopy (Zeiss supra 55) and high-resolution transmission electron microscopy (FEI Tecnai F30). The Seebeck coefficient and electrical conductivity were measured by the simultaneous determination of Seebeck coefficient

and electrical conductivity system (SBA458). The thermal conductivity was measured by transient hot-wire theory method (TC3000) at room-temperature with a reaction time of about 0.2 s. The carrier concentration and mobility were obtained by Van der Pauw Hall measurement (HL5500PC). The output voltages and short-circuit currents of the device were measured in normal atmosphere with Keithley 2400 as a function of the temperature difference between hot and cold sides (Figure S1, Supporting Information). As shown in Figure S1, the temperature gradient was established between the hot source and cooling source, and the temperature was measured with two K-type thermocouples which were gently pressed to the device at the end of the electrodes. Keithley 2400 was used for the  $V_0$  and  $I_s$  testing and all the measurements were computer controlled. The maximum output power ( $P_{\max}$ ) of the tf-TE device defined as  $P_{\max} = V_0 I_s / 4$ , is estimated from the output voltage  $V_0$  and the short-circuit current  $I_s$ . The tf-TE device was also tested as detector by employing the Keithley 2400 which used the continuous monitoring mode with the interval time of 0.1 s.

### **3. Results and discussions**

#### ***Thin films properties***

The X-ray diffraction (XRD) patterns of P-type and N-type  $\text{CoSb}_3$  based thin films are shown in Figure S2 (Supporting Information). The major diffraction peaks of all the samples can be indexed to the body-centered cubic skutterudite phase with space group Im-3 (JCPDS No. 19-0336). No impurity phase can be observed from the diffraction patterns within the detection limit of the XRD spectrometer, indicating that the samples have single skutterudite structure. The lattice parameters were refined using full-profile Rietveld refinement method and the result indicates that the lattice parameter corresponds to that of the pristine  $\text{CoSb}_3$  ( $\sim 9.0344 \text{ \AA}$ ) [36], and it expands to  $\sim 9.0357 \text{ \AA}$  and  $9.0395 \text{ \AA}$  respectively after doping with Ti and In, demonstrating

that the dopant is filling into the crystal structure. The strong peak of the N-type thin film is related to (310) plane and the other peaks are very weak, suggesting a slightly preferential growth along the (310) plane compared with its standard pattern as shown in Figure S2 (Supporting Information). The similar situation can be observed for the P-type thin film. Generally, an intense and sharp peak on XRD pattern is a typical signature for high degree of crystallinity. The crystallite size can be calculated by the Debye-Scherrer equation  $D = 0.9\lambda/\beta\cos\theta$ , where  $D$  is the crystallite size,  $\lambda$  is the wavelength,  $\beta$  is full width half maximum (FWHM) and  $\theta$  is the angle [37]. The thin films contain the nanosized crystallites because the calculated crystallite size is  $\sim 21$  nm for the P-type sample and  $\sim 29$  nm for the N-type sample.

To further confirm the nano-structure of the samples, the surface morphology is observed in Figure S3 (Supporting Information). For the In-doped sample, the grains are distinctly observed and distributed evenly, and the average grain size is less than 50 nm as shown in Figure S3(a). Similarly, globular like nano grains are dispersed throughout the surface for the Ti doped thin film as presented in Figure S3(b). The grains are uniform and the average grain size is around 30 nm. Figure 2 shows the high-resolution images and it implies that both thin films exhibit sphere-like nano grains and the size is below 20 nm which is in good agreement with the XRD result. Hence, the scanning electron microscopy (SEM) and the high-resolution transmission electron microscopy (HRTEM) results prove a high-quality fabrication of  $\text{CoSb}_3$  based nano structured thin films using vacuum sputtering.

Table 1 displays the thermoelectric properties of the thin films, and the optimized performance of the P-type and N-type thin films have been reported in our previous work [35-36]. The Seebeck coefficient  $S$  is negative and the absolute value is  $216 \mu\text{VK}^{-1}$  for the In doped thin film and a positive value of  $125 \mu\text{VK}^{-1}$  is observed for Ti

doped thin film. These results are consistent with the Hall measurements, in which the charge carrier concentration is  $-8.05 \times 10^{20} \text{ cm}^{-3}$  and  $+0.88 \times 10^{20} \text{ cm}^{-3}$ , respectively. Therefore, a prospective thermo-power of the device with one pair of P-N leg is about  $340 \mu\text{VK}^{-1}$ . The doped thin films have very low thermal conductivity  $\kappa$  of  $0.68 \text{ Wm}^{-1}\text{K}^{-1}$  and  $0.51 \text{ Wm}^{-1}\text{K}^{-1}$  due to the dramatic low lattice thermal conductivity  $\kappa_{\text{lat}}$  of  $0.45 \text{ Wm}^{-1}\text{K}^{-1}$  and  $0.43 \text{ Wm}^{-1}\text{K}^{-1}$ , respectively. The main reason explaining such low  $\kappa_{\text{lat}}$  is that the long wavelength phonons are effectively scattered by the nano grains and the short wavelength phonons are scattered by the “rattling” effect of the doping atoms [38-39]. Meanwhile, the dense nanostructure and high crystallinity make the thin films with high charge carrier mobility and an acceptable electrical conductivity. As expected, these two thin films have respectively calculated ZT values of 0.56 and 0.06 at 300 K, which is enhanced to 1.12 and 0.71 at 500 K. These values are already very interesting for flexible device.

### ***Electrode optimization***

In many thin film flexible devices, Au with wonderful character for semiconductors connecting, is commonly used as the electrode material. It is however worth of finding other efficient and low-cost metal electrodes due to the high cost of Au. Herein, four commercial metallic Cu, Al, Mo and Ni layers were introduced by using direct sputtering deposition in our device, which has a single P-N thermocouple. Then the corresponding device performance was investigated. Figure 3 shows the open output voltage ( $V_o$ ) and short-circuit current ( $I_s$ ) of the tf-TE device with various electrodes as function of temperature difference  $\Delta T$ . The temperature gradient being imposed parallel to the length of the tf-TE leg. Herein, the temperature of cold and hot side was measured by the two K-type thermocouples which were gently pressed to the device at the end of the electrodes. Figure 3 (a) reveals that the  $V_o$  of all devices

increases linearly with increasing temperature difference, except for the Cu electrode-based device with rapidly decreasing  $V_o$  when the temperature difference reaches higher than 190 K. Though the  $V_o$  of the device with Al electrode has high value, it has extremely low  $I_s$  as shown in Figure 3 (b), suggesting high electric losses likely due to the large contact resistance. Similarly, despite the highest  $V_o$  of the device with Ni layer, its  $I_s$  is very low. Those results indicate that Al and Ni are not suitable as the matched electrode material in our TE thin films. The linear fit of the experimental data yields a Seebeck coefficient of  $348 \mu\text{VK}^{-1}$  and  $335 \mu\text{VK}^{-1}$  of the devices with Cu and Mo electrode, which agrees well with the value for the PN junction of about  $340 \mu\text{VK}^{-1}$ . The  $V_o$  and  $I_s$  of the devices with Cu and Mo is thermally steady, especially with Mo, which keeps the increasing trend at the whole temperature range. Even though the device with Cu electrode has higher  $I_s$ , but it drops with the  $V_o$  at higher temperature difference because of its oxidation in air and diffusion effect, leading to electric losses due to the increasing thermal and contact resistance.

After analyzing the device performance based on those electrode materials, it can be deduced that the Cu is the best electrode for matching the  $\text{CoSb}_3$  based TE materials, but the device deteriorates in use in air atmosphere at high temperature. To address this challenge, a multilayer electrode structure is proposed. A nano thickness Ni or Mo was deposited as the buffer to prevent the inter-diffusion of the Cu and TE material. It is also deposited on the surface of the Cu layer as a protection against the oxidation in air. Figure 4 (a) and (b) show the influence of the Ni thickness on the  $V_o$  and  $I_s$  of the device and Figure 4 (c) display the calculated  $P_{\text{max}}$ . Comparing with the device with single Cu electrode layer, the  $V_o$  and  $I_s$  of the device using the 5 nm Ni layer have been slightly improved, suggesting that the multilayer electrode structure is valid for

matching the TE thin films. However, the  $V_o$  and  $I_s$  decrease obviously when the Ni thickness increases. Especially, the  $P_{max}$  of the device shows a four-time drop when the Ni thickness increases from 5 nm to 20 nm (Figure 4 c). Unlike the Ni-Cu-Ni multilayer, the device with Mo-Cu-Mo multilayer electrode structure can generate larger open circuit voltage above 90 mV with increasing Mo thickness (Figure 4 d). And all the  $V_o$  show approximately linear increase with increasing temperature difference, which implies that  $S$  remains constant under the test temperature. Though the  $I_s$  has slightly decreased when the Mo thickness increases as shown in Figure 4 (e), it keeps a linear increase during the measurement. The temperature stability of both  $V_o$  and  $I_s$  of the device with Mo-Cu-Mo electrode structure is particularly important for practical use. The calculated  $P_{max}$  values of the device with the Mo-Cu-Mo electrode are shown in Figure 4 (f). The highest  $P_{max}$  value is obtained by using the Mo thickness of 10 nm and the maximum value is 13.9  $\mu$ W at  $\Delta T = 210$  K, which is about two times larger than that of the device with single Cu electrode. This implies that the electrical contact resistance decreases after applying the multilayer electrode structure, leading to greatly enhanced performance of tf-TE device. It is worth noting that the cross-section area of the device with single PN thermocouple, including the flexible substrate, is about 0.03  $\text{cm}^2$ . Thus, the power density can be as high as 0.46  $\text{mW}/\text{cm}^2$ , which is comparable to those of the previously reported of f-TE device [11-13, 40, 41]. Furthermore, if we calculate the power density within the TE thin films, it clearly demonstrates that the power density value will be one order of magnitude higher due to the small thickness of the TE thin film, which is only 5 % of the flexible substrate. The Key facts responsible for these improvements are the use of  $\text{CoSb}_3$  nano thin films with a high ZT as the raw materials and the use of multilayer-electrode structure, leading to a significant reduction of the contact

resistance between the TE thin films and solder materials.

### ***Device performance***

In order to investigate the reliability and the repeatability of the devices, we monitored the testing cycles in air atmosphere and Figure 5 shows the  $P_{\max}$  of the device as function of temperature difference for different electrode configurations: (a) Ni-Cu-Ni with the Ni thickness of 5 nm, (b) Mo-Cu-Mo with the Mo thickness of 5 nm and (c) Mo with a thickness of 10 nm. It can be seen from Figure 5 (a) that the  $P_{\max}$  of the tf-TE device with the Ni-Cu-Ni electrode, exhibits noticeable degradation and suffers a output power loss of about 50 % after the third cycle, indicating that the device has poor thermal stability. Fortunately, the device with the Mo-Cu-Mo electrode structure is stable. Especially the device with the thinner Mo thickness demonstrates a constant  $P_{\max}$  even after several cycles. Furthermore, Figure 5 (d) shows the output power versus the current produced by a single thermocouple or two thermocouples by using the Mo layer with 5 nm thickness and a constant temperature difference of 210 K. With an decrease in load resistance, the current increases and hence a maximum output power can be observed with a current around 0.35 mA. The maximum current of the device with two thermocouples is slightly smaller than that of one thermocouple, indicating the increase of internal resistance which might cause by the asymmetry of the materials. The  $P_{\max}$  doubles after doubling the number of the thermocouples, suggesting that a promising tf-TE device with high thermal stability and possibility using it in air atmosphere is obtained after the optimization of the electrode. This result is particularly interesting for low temperature tf-TE generator applications exploiting various practically available heat sources.

The developed  $\text{CoSb}_3$  based nano thin films exhibit relatively high Seebeck coefficient and they may also have high thermal sensitivity due to the high carrier

mobility, which is favorable for thermal detector applications. Therefore, a thermal detector device, shown in Figure 6 (a) and based on this thermoelectric material, has been tested as a proof of concept. The continuous response of a single thermocouple tf-TE device was measured for six cycles and eleven cycles with respective 10 s and 5 s interval between two events with the finger touching the region of the electrode contact as “on” and finger removed as “off”. The output signals of the single thermocouple device are shown in Figure 6 (b) and (c). It can be seen that the voltage increases rapidly in response to the “on” state. The rise time of all the “on” events is below 1 s, indicating that the detector has a fast response. The device also has stable maximum output voltage about 0.65 mV, suggesting that the thermal gradient is about 2 K at the ambient temperature of about 300 K. Figure 6 (d) and (e) displays the voltage response of the tf-TE device with two thermocouples, where an identical “on-off” process is applied. However, the maximum voltage has enhanced to about 1.08 mV, which is a significant improvement compared to that of single thermocouple. The output value is slightly smaller than 2 times of the value for the single thermocouple. Such marginally decreased response is attributed to the insufficient thermal contact area of the finger. Moreover, the response time still maintains at a level of a few hundreds of milliseconds, indicating more optimized thermoelectric conversion. Therefore, our tf-TE device can be considered for use as sensor for fast/real-time human touch electrical trigger/detector with milliseconds reaction time. Generally, the tf-TE device is considered for low-power source application, but it can also have a huge potential for large-scale power source. For instance, we fabricated a module with 100 identical PN thermocouples, which were connected in series to form an one dimensional array. The structure of this tf-TE generator is shown in Figure 7 (a) and the PN couples were connected by the metal layer bonding (the thickness is less

than 5 mm). The insulating ceramic rods were used for fixing the couples. One stainless steel plate covering the top is used for heat absorption and another one on the bottom is used as heat diffuser. The picture of the real product is shown in the Figure 7 (b). Figure 7 (c) shows the thermoelectric properties of the generator. The maximum output voltage is about 7 V and the maximum output power is about 1.1 mW at the temperature difference of 210 K. The power produced per couple and per unit temperature difference is 11  $\mu\text{W/K-couple}$ , roughly in line with the value of a P-N couple. The calculated power density is about  $0.07 \text{ mWcm}^{-2}$  (the surface area is about  $15 \text{ cm}^2$ ). It still shows a great potential for further improvement by optimizing certain parameters of this device, such as the thickness and the length-width ratio of the TE thin films, the structure of the device.

## **Conclusions**

In this work, we have demonstrated that  $\text{CoSb}_3$  based nano thin film with high ZT value even at low temperature can be obtained with both P and N types by appropriate doping of In and Ti respectively. This achievement has allowed fabricating high-performance thin film devices, which can operate under near ambient conditions. Meanwhile, the stable Seebeck coefficient and enhanced ZT value of  $\text{CoSb}_3$  nano thin films, are highly favorable for increasing the output voltage and the responsivity of the flexible device. Another important result of this work is related to the optimization of the electrode by using a multilayer structure, providing dramatically enhanced performance of the thin film thermal electric device, especially the electrical transport and the thermal stability in air atmosphere. As a result, over 90 mV output voltage of a single thermocouple was generated at temperature difference of 210 K, which is even superior to the commercial bulk device. The power density of a single couple device is  $0.46 \text{ mW/cm}^2$  and it would be one order of magnitude higher if only the thin

film, excluding the substrate, is considered. In this case, the power density would be much higher than that of other reported thin film devices. Moreover, the thin-film thermoelectric device also exhibits fast responsivity, with a reaction time of a few hundreds of milliseconds, as well as high stability. It has also been demonstrated the possibility of obtaining relatively high output voltage of about 7 V at a current intensity of about 0.35 mA with these thin film thermoelectric devices. These results are expected to have practical applications that can generate electricity anywhere to activate portable electronic devices and sensing owing to its excellent environmental adaptability.

### **Supporting information**

Detailed experimental section, device measurement, XRD analysis, and SEM morphology (PDF).

### **Notes**

The authors declare no competing financial interest.

### **Acknowledgments**

This work was supported by the National Natural Science Foundation of China (Grant No. 11604212), Guangdong Basic and Applied Basic Research Foundation (2020A1515010515), Shenzhen Key Lab Fund (ZDSYS 20170228105421966).

### **References**

[1]. Shi, X. L.; Zou, J.; Chen, Z. G. Advanced thermoelectric design: from materials and structures to devices. *Chemical reviews* **2020**, 120, 7399-7515.

- [2]. Shi, X. L.; Chen, W. Y.; Zhang, T.; Zou, J.; Chen, Z. G. Fiber-based Thermoelectrics for Solid, Portable, and Wearable Electronics. *Energy Environ. Sci.* **2021**, 14, 729-764.
- [3]. Peng, Y.; Lai, H. J.; Liu, C. Y.; Gao, J.; Kurosawa, M.; Nakatsuka, O.; Takeuchi, T.; Zaima, S.; Tanemura, S.; Miao, L. Realizing high thermoelectric performance in p-type  $\text{Si}_{1-x-y}\text{Ge}_x\text{Sn}_y$  thin films at ambient temperature by Sn modulation doping. *Appl. Phys. Lett.* **2020**, 117, 053903.
- [4]. Gao, J.; Miao, L.; Liu, C. Y.; Wang, X. Y.; Peng, Y.; Wei, X. Y.; Zhou, J. H.; Chen, Y.; Hashimoto, R.; Asaka, T.; Koumoto, K. A novel glass-fiber-aided cold-press method for fabrication of n-type  $\text{Ag}_2\text{Te}$  nanowires thermoelectric film on flexible Copy-paper Substrate. *J. Mater. Chem. A* **2017**, 5, 24740-24748.
- [5]. Kim, S. J.; We, J. H.; Cho, B. J. A wearable thermoelectric generator fabricated on a glass fabric. *Energy & Environmental Science* **2014**, 7, 1959-1965.
- [6]. Culebras, M.; Cho, C.; Kreckler, M.; Smith, R.; Song, Y. X.; Gomez, C. M.; Cantarero, A.; Grunlan, J. C. High thermoelectric power factor organic thin films through combination of nanotube multilayer assembly and electrochemical polymerization. *ACS applied materials & interfaces* **2017**, 9, 6306-6313.
- [7]. Chen, Y. X.; Shi, X. L.; Zheng, Z. H.; Li, F.; Liu, W. D.; Chen, W. Y.; Li, X. R.; Liang, G. X.; Luo, J. T.; Fan, P.; Chen, Z. G. Two-dimensional  $\text{WSe}_2/\text{SnSe}$  p-n junctions secure ultrahigh thermoelectric performance in n-type Pb/I Co-doped polycrystalline SnSe. *Mater. Today Phys.* **2021**, 16, 100306.
- [8]. Fan, P.; Huang, X. L.; Chen, T. B.; Li, F.; Chen, Y. X.; Jabar, B.; Chen, S.; Ma, H. L.; Liang, G. X.; Luo, J. T.; Zhang, X. H.; Zheng, Z. H.  $\alpha\text{-Cu}_2\text{Se}$  thermoelectric thin films prepared by copper sputtering into selenium precursor layers. *Chem. Eng. J.* **2021**, 410, 128444.

- [9]. Li, J.; Zhang, X. Y.; Chen, Z. W.; Lin, S. Q.; Li, W.; Shen, J. H.; Witting, I. T.; Faghaninia, A.; Chen, Y.; Jain, A.; Chen, L. D.; Snyder, G. J.; Pei, Y. Z. Low-symmetry rhombohedral GeTe thermoelectrics. *Joule* **2018**, *2*, 976-987.
- [10]. Nunna, R.; Qiu, P. F.; Yin, M. J.; Chen, H. Y.; Hanus, R.; Song, Q. F.; Zhang, T. S.; Chou, M. Y.; Agne, M. T.; He, J. Q.; Snyder, G. J.; Shi, X.; Chen, L. D. Ultrahigh thermoelectric performance in Cu<sub>2</sub>Se-based hybrid materials with highly dispersed molecular CNTs. *Energy & Environmental Science* **2017**, *10*, 1928-1935.
- [11]. Wang, Y.; Yang, L.; Shi, X. L.; Shi, X.; Chen, L. D.; Dargusch, M. S.; Zou, J.; Chen, Z. G. Flexible thermoelectric materials and generators: challenges and innovations. *Advanced materials* **2019**, *31*, 1807916.
- [12]. Lu, Y.; Ding, Y. F.; Qiu, Y.; Cai, K. F.; Yao, Q.; Song, H. J.; Tong, L.; He, J. Q.; Chen, L. D. Good Performance and Flexible PEDOT:PSS/Cu<sub>2</sub>Se Nanowire Thermoelectric Composite Films. *ACS applied materials & interfaces* **2019**, *11*, 12819-12829.
- [13]. Jiang, C.; Ding, Y. F.; Cai, K. F.; Tong, L.; Lu, Y.; Zhao, W. Y.; Wei, P. Ultrahigh Performance of n-Type Ag<sub>2</sub>Se Films for Flexible Thermoelectric Power Generators. *ACS applied materials & interfaces* **2020**, *12*, 9646-9655.
- [14]. Jin, Q.; Jiang, S.; Zhao, Y.; Wang, D.; Qiu, J. H.; Tang, D. M.; Tan, J.; Sun, D. M.; Hou, P. X.; Chen, X. Q.; Tai, K. P.; Gao, N.; Liu, C.; Cheng, H. M.; Jiang, X. Flexible layer-structured Bi<sub>2</sub>Te<sub>3</sub> thermoelectric on a carbon nanotube scaffold. *Nature materials* **2019**, *18*, 62-68.
- [15]. Venkatasubramanian, R.; Siivola, E.; Colpitts, T.; O'Quinn, B. Thin-film thermoelectric devices with high room-temperature figures of merit. *Nature* **2001**, *413*, 597-602.

- [16]. Hicks, L. D.; Dresslhaus, M. S. Effect of quantum-well structures on the thermoelectric figure of merit. *Phys. Rev. B* **1993**, *47*, 12727.
- [17]. Bulman, G.; Barletta, P.; Lewis, J.; Baldasaro, N.; Manno, M.; Cohen, A. B.; Yang, B. Superlattice-based thin-film thermoelectric modules with high cooling fluxes. *Nat. Commun.* **2016**, *7*, 10302.
- [18]. Ding, D. F.; Wang, D. W.; Zhao, M.; Lv, J. W.; Jiang, H. ; Lu, C. G.; Tang, Z. Y. Interface Engineering in Solution - Processed Nanocrystal Thin Films for Improved Thermoelectric Performance. *Adv. Mater.* **2016**, *31*, 1603444.
- [19]. Chowdhury, I.; Prasher, R.; Lofgreen, K.; Chrysler, G.; Narasimhan, S.; Mahajan, R.; Koester, D.; Alley, R.; Venkatasubramanian, R. On-chip cooling by superlattice-based thin-film thermoelectrics. *Nat. Nanotechnol.* **2009**, *4* , 235-238.
- [20]. Tian, R. M.; Wan, C. L.; Wang, Y. F.; Wei, Q. S.; Ishida, T.; Yamamoto, A.; Tsuruta, A.; Shin, W.; Li, S.; Koumoto, K. A solution-processed TiS<sub>2</sub>/organic hybrid superlattice film towards flexible thermoelectric devices. *J. Mater. Chem. A* **2017**, *5*, 564-570.
- [21]. Yadav, A.; Pipe, K. P.; Shtein, M. Fiber-based flexible thermoelectric power generator. *J. Power Sou.* **2008**, *175*, 909-913.
- [22]. Szobolovszky, R.; Siffalovic, P.; Hodas, M.; Pelletta, M.; Jergel, M.; Sabol, D.; Macha, M.; Majkova, E. Waste heat recovery in solid-state lighting based on thin film thermoelectric generators. *Sus. Energy Technol. Ass.* **2016**, *18*, 1-5.
- [23]. Zhu, W.; Deng, Y.; Cao, L. L. Light-concentrated solar generator and sensor based on flexible thin-film thermoelectric device. *Nano Energy* **2017**, *34*, 463-471.
- [24]. Pan, Y.; Tagliabue, G.; Eghlidi, H.; Höller, C.; Dröscher, S.; Hong, G.; Poulidakos, D. A rapid response thin-film plasmonic-thermoelectric light detector.

*Sci. Rep.* **2016**, 6, 37564.

- [25]. Savage, N. Thermoelectric coolers, Thermoelectric coolers. *Nat. Photon.* **2009**, 3, 541-542.
- [26]. Liu, Z. Y.; Zhu, J. L.; Tong, X.; Niu, S.; Zhao, W. Y. A review of CoSb<sub>3</sub>-based skutterudite thermoelectric materials. *Journal of Advanced Ceramics* **2020**, 9, 647-673.
- [27]. Bourgès, C.; Sato, N.; Baba, T.; Baba, T.; Ohkubo, I.; Tsujii, N.; Mori, T. Drastic power factor improvement by Te doping of rare earth-free CoSb<sub>3</sub>-skutterudite thin films. *RSC Advances* **2020**, 10, 21129-21135.
- [28]. Qin, D. D.; Wu, H. J.; Cai, S. T.; Zhu, J. B.; Cui, B.; Yin, L.; Qin, H. X.; Shi, W. J.; Zhang, Y.; Zhang, Q.; Liu, W. S.; Cao, J.; Pennycook, S. J.; Cai, W.; Sui, J. H. Enhanced Thermoelectric and Mechanical Properties in Yb<sub>0.3</sub>Co<sub>4</sub>Sb<sub>12</sub> with In Situ Formed CoSi Nanoprecipitates. *Advanced Energy Materials* **2019**, 9, 1902435.
- [29]. Masarrat, A.; Bhogra, A.; Meena, R.; Bala, M.; Singh, R.; Barwal, V.; Dong, C. L.; Chen, C. L.; Som, T.; Kumar, A.; Niazi, A.; Asokan, K. Effect of Fe ion implantation on the thermoelectric properties and electronic structures of CoSb<sub>3</sub> thin films. *RSC Advances* **2019**, 9, 36113-36122.
- [30]. Bhardwaj, R.; Gahtori, B.; Johari, K. K.; Bathula, S.; Chauhan, N. S.; Vishwakarma, A.; Dhakate, S. R.; Auluck, S.; Dhar, A. Collective Effect of Fe and Se To Improve the Thermoelectric Performance of Unfilled p-Type CoSb<sub>3</sub> Skutterudites. *ACS Applied Energy Materials* **2019**, 2, 1067-1076.
- [31]. Ortiz, B. R.; Crawford, C. M.; McKinney, R. W.; Parilla, P. A.; Toberer, E. S. Thermoelectric properties of bromine filled CoSb<sub>3</sub> skutterudite. *Journal of Materials Chemistry A* **2016**, 4, 8444-8450.
- [32]. Duan, B.; Yang, J.; Salvador, J. R.; He, Y.; Zhao, B.; Wang, S. Y.; Wei, P.;

- Ohuchi, F. S.; Zhang, W. Q.; Hermann, R. P.; Gourdon, O.; Mao, S. X.; Cheng, Y. W.; Wang, C. M.; Liu, J.; Zhai, P. C.; Tang, X. F.; Zhang, Q. J.; Yang, J. H. Electronegative guests in CoSb<sub>3</sub>. *Energy & Environmental Science* **2016**, 9, 2090-2098.
- [33]. Rogl, G.; Grytsiv, A.; Yubuta, K.; Puchegger, S.; Bauer, E.; Raju, C.; Mallik, R. C.; Rogl, P. In-doped multifilled n-type skutterudites with ZT= 1.8. *Acta Materialia* **2015**, 95, 201-211.
- [34]. Daniel, M. V.; Lindort, M.; Albrecht, M. Thermoelectric properties of skutterudite CoSb<sub>3</sub> thin films. *Journal of applied physics* **2016**, 120, 125306.
- [35]. Zheng, Z. H.; Fan, P.; Zhang, Y.; Luo, J. T.; Huang, Y.; Liang, G. X. High-performance In filled CoSb<sub>3</sub> nano thin films fabricated by multi-step co-sputtering method. *Journal of Alloys and Compounds* **2015**, 639, 74-78.
- [36]. Liang, G. X.; Zheng, Z. H.; Li, F.; Luo, J. T.; Jin, H.; Zhang, X. H.; Fan, P. Nano structure Ti-doped skutterudite CoSb<sub>3</sub> thin films through layer inter-diffusion for enhanced thermoelectric properties. *Journal of the European Ceramic Society* **2019**, 39, 4842-4849.
- [37]. Fan, P.; Wei, M.; Zheng, Z. H.; Zhang, X. H.; Ma, H. L.; Luo, J. T.; Liang, G. X. Effects of Ag-doped content on the microstructure and thermoelectric properties of CoSb<sub>3</sub> thin films. *Thin Solid Films* **2019**, 679, 49-54.
- [38]. Ren, W.; Sun, Y.; Zhang, J. L.; Xia, Y. P.; Geng, H. Y.; Zhang, L. X. Doping distribution in Skutterudites with ultra-high filling fractions for achieving ultra-low thermal conductivity. *Acta Materialia* **2021**, 209, 116791.
- [39]. Zheng, Z. H.; Shi, X. L.; Ao, D. W.; Liu, W. D.; Chen, Y. X.; Li, F.; Chen, S.; Tian, X. Q.; Li, X. R.; Duan, J. Y.; Ma, H. L.; Zhang, X. H.; Liang, G. X.; Fan, P.; Chen, Z. G. Rational band engineering and structural manipulations inducing high

thermoelectric performance in n-type CoSb<sub>3</sub> thin films. *Nano Energy* **2021**, 81, 105683.

[40]. Park, N. W.; Ahn, J. Y.; Park, T. H.; Lee, J. H.; Lee, W. Y.; Cho, K.; Yoon, Y. G.; Choi, C. J.; Park, J. S.; Lee, S. K. Control of phonon transport by the formation of the Al<sub>2</sub>O<sub>3</sub> interlayer in Al<sub>2</sub>O<sub>3</sub>–ZnO superlattice thin films and their in-plane thermoelectric energy generator performance. *Nanoscale* **2017**, 9, 7027-7036.

[41]. Kim, S. J.; Lee, H. E.; Choi, H.; Kim, Y. J.; We, J. H.; Shin, J. S.; Lee, K. J.; Cho, B. J. High-performance flexible thermoelectric power generator using laser multiscanning lift-off process. *ACS Nano* **2016**, 10, 10851-10857.

## Figure Caption

**Figure 1** Schematic of the flexible CoSb<sub>3</sub> nano thin film thermoelectric device fabricated. (a) multilayer method for preparing N-type In doped CoSb<sub>3</sub> nano thin film, (b) precursor Ti nano thickness layer for preparing P-type CoSb<sub>3</sub> nano thin film, (c) electrode optimization of the device, (d) photo of the device.

**Figure 2** HRTEM images of the thin films (a) N-type In doped CoSb<sub>3</sub>, (b) P-type CoSb<sub>3</sub>.

**Figure 3** (a) Open output voltage and (b) short-circuit current for devices with various electrodes as function of applied temperature difference.

**Figure 4** The influence of the thickness of the Ni and Mo layer on the thermoelectric properties of the device. (a) open output voltage of the Ni-Cu-Ni electrode, (b) short-circuit current of the Ni-Cu-Ni electrode, (c) output maximum power of the Ni-Cu-Ni electrode, (d) open output voltage of the Mo-Cu-Mo electrode, (e) short-circuit current of the Mo-Cu-Mo electrode, (f) output maximum power of the Mo-Cu-Mo electrode.

**Figure 5** The reliability and repeatability measurements of the device (a)  $P_{\max}$  of the device with Ni-Cu-Ni electrode, (b)  $P_{\max}$  of the device with Mo-Cu-Mo electrode of Mo thickness of 5 nm, (c)  $P_{\max}$  of the device with Mo-Cu-Mo electrode of Mo thickness of 10 nm, (d) the output power of single thermocouple and double thermocouples with the Mo layer thickness of 5 nm as a function of applied temperature difference.

**Figure 6** Time evolution of output voltage of the thermoelectric device with the finger

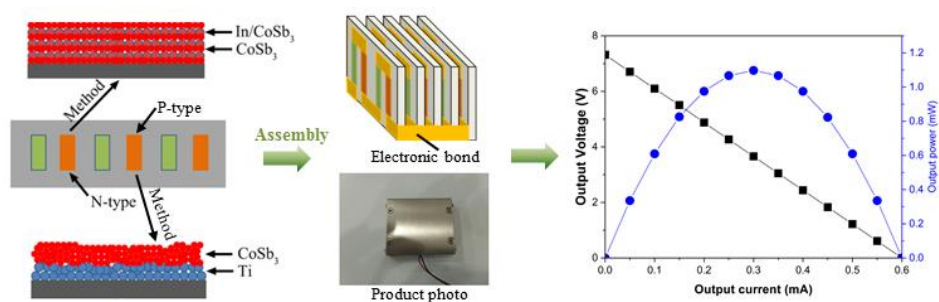
touching instantly the contact/electrode. (a) the measurement schematic illustration, (b) six cycles with 10 s interval time of a single thermocouple, (c) eleven cycles with 5 s interval time of a single thermocouple, (d) six cycles with 10 s interval time of two thermocouples (e) eleven cycles with 5 s interval time of two thermocouples.

**Figure 7** (a) and (b) Schematic and device photo of the thermoelectric module, (c) the output power as a function of applied temperature difference.

Table 1 electric and thermoelectric properties of the thin films

	$\mu$ ( $\text{cm}^2/\text{V}\cdot\text{S}$ )	$n$ ( $\times 10^{20} \text{ cm}^{-3}$ )	$\sigma$ ( $\times 10^4 \text{ S/m}$ )	$S$ ( $\mu\text{VK}^{-1}$ )	$\kappa/\kappa_{\text{lat}}$ ( $\text{Wm}^{-1}\text{K}^{-1}$ )	ZT (300 K/500 K)
N-type	1.75	-8.05	2.7	-216	0.68/0.45	0.56/1.12
P-type	2.84	0.88	0.7	125	0.51/0.43	0.06/0.71

## Table of Contents (TOC) graphic



## Graphic for manuscript

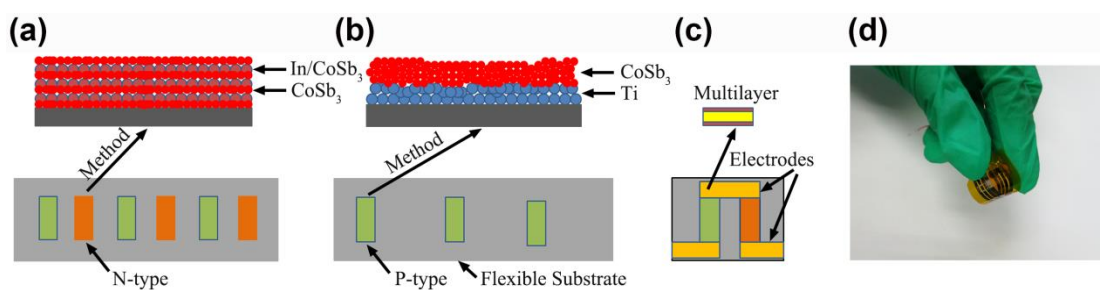


Figure 1

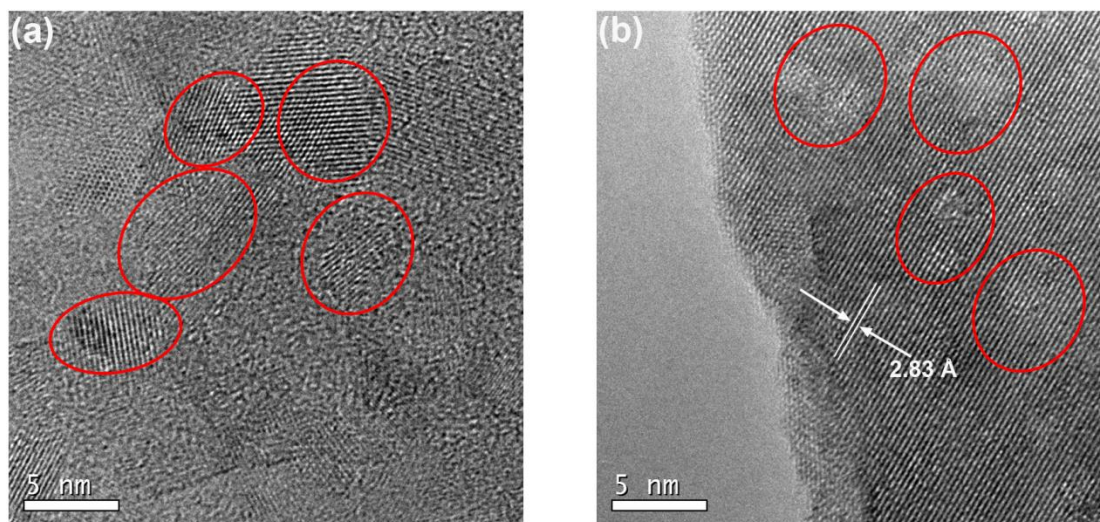


Figure 2

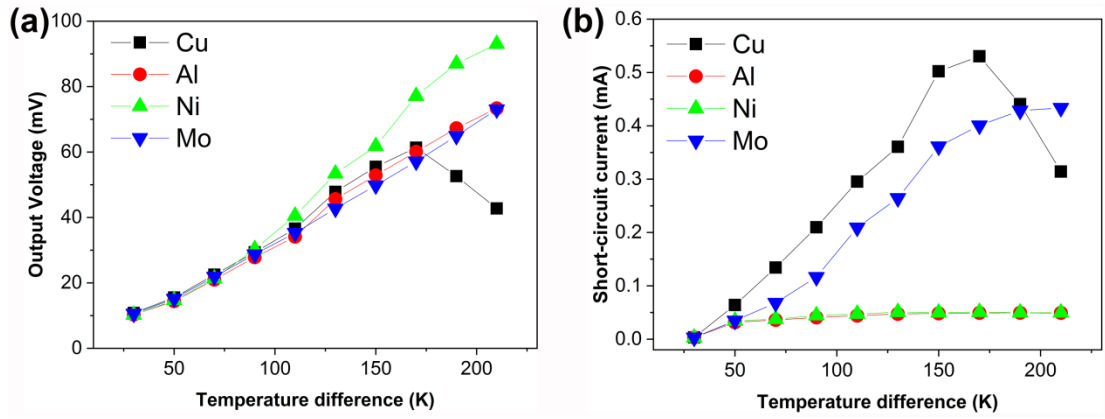


Figure 3

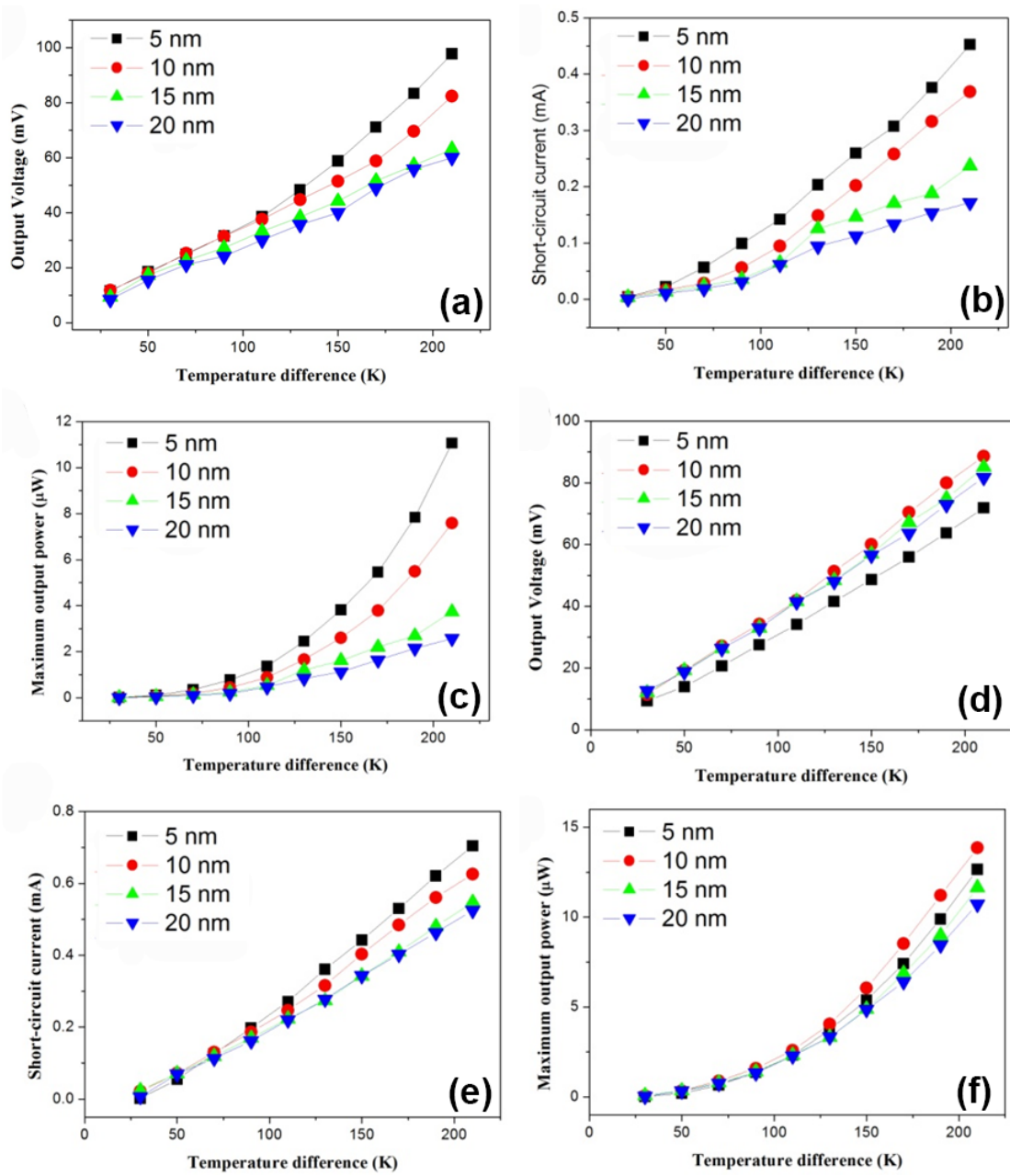


Figure 4

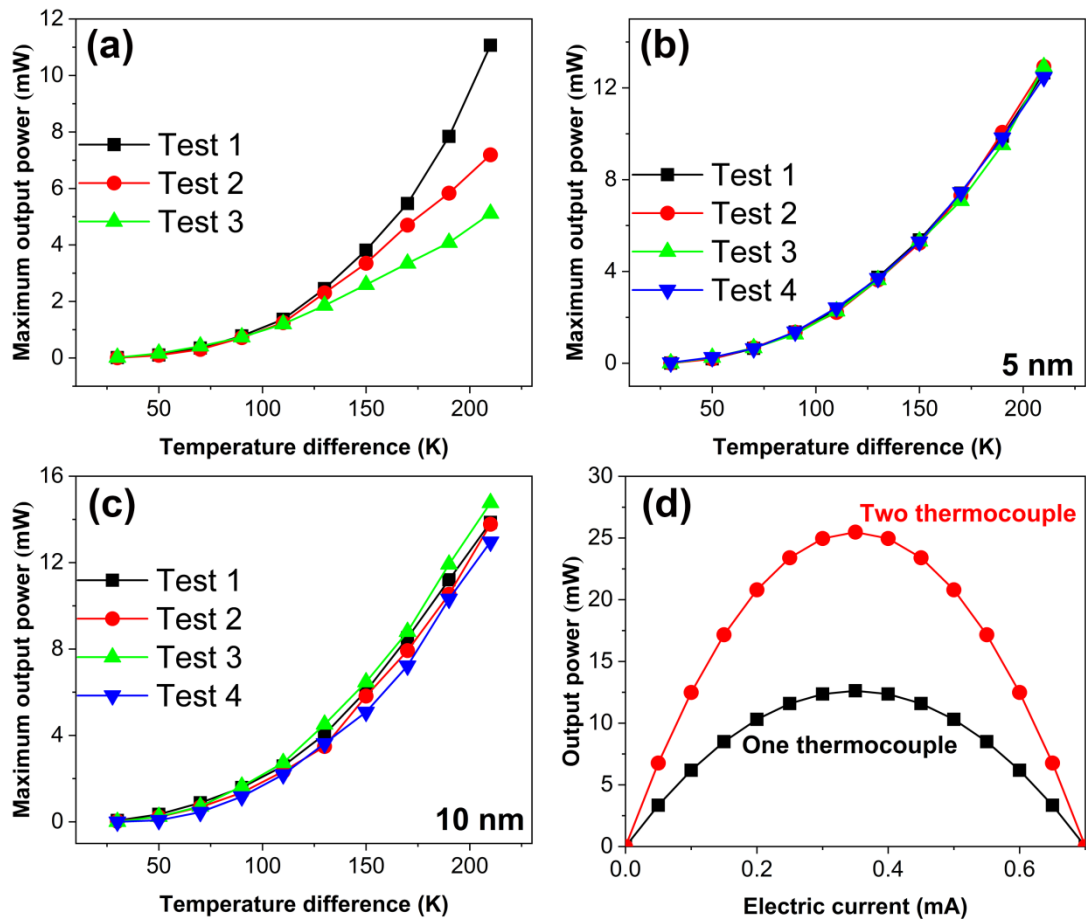


Figure 5

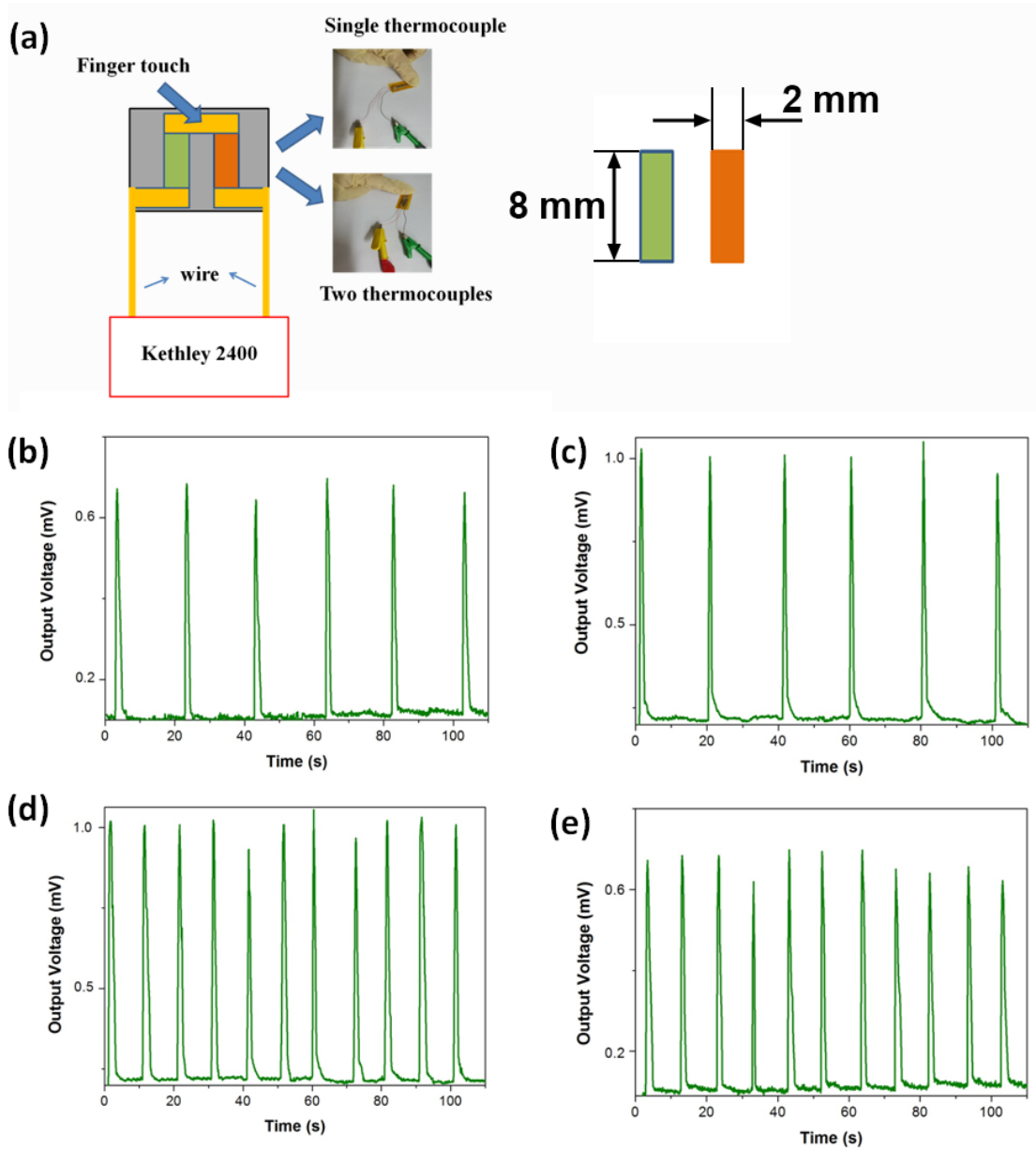


Figure 6

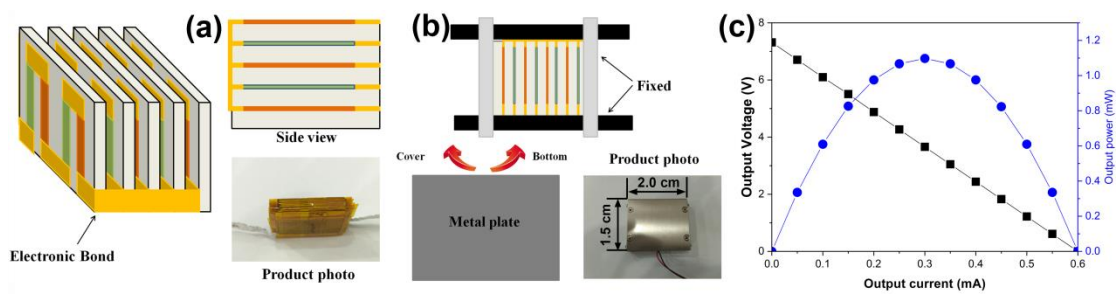


Figure 7